

# HIGH ENERGY PHYSICS

## Measuring the Lifetime of Cosmic-Ray Muons

Guilherme H. Caumo (260964615)

McGill University Department of Physics

November 1, 2024

---

### Abstract

This study used a setup of plastic scintillation detectors and iron stopping media to measure the lifetime of cosmic-ray muons at sea level. The lifetime was calculated by measuring the delay between muon captures by the stopping media and the detection of emitted electrons resulting from the decay process. Thereafter, the data were analyzed by calculating the lifetime from the distribution of measured muon delays using an exponential fit. Based on this, it was observed that the measured value,  $\tau = 2.18 \pm 0.3 \mu\text{s}$ , agrees with the accepted values for the lifetime of muons,  $\tau = 2.1969811 \pm 0.0000022 \mu\text{s}$ , within  $1 \sigma$ . In sum, this study successfully measured the mean lifetime of cosmic-ray muons, though future experiments should aim to achieve greater experimental accuracy and expand upon methods presented here to explore more properties of elementary particles.

---

# 1 Introduction

## 1.1 Theory

In 1937, C. W. Anderson and S. H. Neddermeyer made a breakthrough in particle physics with the discovery of the muon by exposing a cloud chamber to cosmic-rays [1]. Cosmic-ray muons,  $\mu^-$  and  $\mu^+$ , are created in the upper atmosphere when high-energy cosmic-rays interact with the nuclei of atmospheric particles, a process that produces pi-mesons,  $\pi^+$  and  $\pi^-$ , which in turn produce muons via their decays [2], such that:

$$\begin{aligned}\pi^+ &\longrightarrow \mu^+ + \nu \\ \pi^- &\longrightarrow \mu^- + \bar{\nu},\end{aligned}\tag{1}$$

where  $\nu$  represents a neutrino and  $\bar{\nu}$  an anti-neutrino. Muons are highly penetrative particles born in "cascades" in the upper atmosphere, and survive long enough to reach sea level [3]. Muons, like electrons, interact via weak and electromagnetic (EM) forces and, consequently, have less chance of being absorbed than pions [3] [4]. In addition, muons are less susceptible to losing energy due to EM radiation processes than electrons by having a mass 207 times greater [3] [5].

Muons then decay through weak interactions into an electron or a positron, respectively, as well as two pairs of neutrinos, such that:

$$\begin{aligned}\mu^- &\longrightarrow e^- + \bar{\nu}_e + \nu_\mu \\ \mu^+ &\longrightarrow e^+ + \nu_e + \bar{\nu}_\mu,\end{aligned}\tag{2}$$

where  $\mu^-$  represents the muon,  $e^-$  represents the electron,  $\bar{\nu}_e$  represents the electron anti-neutrino, and  $\nu_\mu$  represents the muon neutrino while  $\mu^+$ ,  $e^+$ ,  $\nu_e$ , and  $\bar{\nu}_\mu$  represent the respective anti-particles [6]. Furthermore, the process of muon decay can be assigned a characteristic lifetime,  $\tau = 2.1969811 \pm 0.0000022 \mu\text{s}$ , that is defined as the time elapsed until a population of particles is reduced by a factor of  $e$  [6]. Hence, the governing equation for the decay

process is:

$$I(t) = I_o e^{-t/\tau}, \quad (3)$$

where the approximate expected flux of muons at sea level,  $I(t)$ , is given by the travel time from the initial height in the upper atmosphere,  $t$ , the mean lifetime,  $\tau$ , and the expected flux of muons in the initial height,  $I_o$ .

## 1.2 Muon Absorption

Before decaying, however, a muon has a chance of being absorbed by ordinary matter. In more detail, muon absorption occurs when a negative muon is captured by a proton, producing a neutron and a neutrino [7], such that:

$$\mu^- + p \longrightarrow n + \nu_\mu. \quad (4)$$

The probability of a muon being absorbed by an atomic nucleus is proportional to the number of atomic electrons of the stopping material [8]. Consequently, it can be noted that iron ( $Z = 26$ ), or steel, would make for an effective and readily available material to act as a stopping medium. In contrast, a material such as carbon ( $Z = 6$ ) could be featured in the detector apparatus as the number of muons stopping in such a detector would be much smaller.

## 1.3 Experimental Goals

Considering the points above, this study aims to use a setup of photomultiplier tubes (PMTs) attached to plastic scintillators and steel blocks to measure the lifetime of cosmic-ray muons, owing to the fundamental role this phenomenon plays in the study of particle physics.

# 2 Methodology

## 2.1 Equipment and Calibration

Firstly, the methodology of this experiment featured the use of three detectors, labeled A, B, and C, with each detector composed of a plastic scintillator glued to a PMT. Scintillator ma-

materials are luminescent and emit light when struck by charged particles. Plastic scintillators are well-established in the literature for having uses in experimental setups involving charged particles [9]. Each scintillator (28.4 cm x 10.5 cm x 2.83 cm) was wrapped in black tape to keep scintillated photons within the apparatus and prevent other light sources from affecting the experiment. Moreover, the PMT functions as a high-vacuum tube that multiplies currents produced by incident light [9]. Each PMT used in this setup has a Cockroft-Walton voltage multiplier attached to its base, which provides the necessary high voltage needed for the PMT to function and multiplies the voltages by a factor of 100, while also providing the output signal. The output trace is read by a SDS1204X-E SIGLENT oscilloscope connected to a laptop, which records the data through a Python program.

Secondly, the calibration for this setup was done by stacking the detectors on top of each other and placing the detector being calibrated in between the other two. Traces from the detector being calibrated were then recorded at four different voltages (15V, 16V, 17V, and 18V) while the passage of a muon was given by the existence of a signal in the other two detectors. Thereafter, the traces recorded by the detectors were integrated to obtain the distribution of the charges for each of the tested voltages, as seen in the sample trace shown in Figure 1. This process was possible since the voltages of the traces were divided by the 50  $\Omega$  input impedance of a terminator placed at the oscilloscope's channel input, which converted the voltages into currents. Consequently, the values of current,  $i$ , in milliamps were used to calculate the trace charges,  $Q$ , in picocoulombs due to the following relation:

$$Q = \int i dt, \quad (5)$$

where  $dt$  represents the period of time being integrated in nanoseconds.

Finally, Moyal curves were graphed over these distributions, and the mean values were extracted as seen in Figure 2. These mean values were then graphed, and a parabola was fitted to the data points. The resulting parabola fit was then used to obtain the high voltage value associated with a mean charge of 1.75 pC (see Appendix A for parabola fits). This process was repeated for every detector used in this experiment, with the final voltages being  $16.9 \pm 0.02$  V for detector A,  $17.9 \pm 0.02$  V for detector B, and  $15.6 \pm 0.03$  V for detector

C.

This calibration process was necessary to equalize each detector's response. In the event that the voltage applied to the PMTs was too low, the apparatus would not be fully efficient [10]. On the other hand, applying excessive voltage would stress the PMTs unnecessarily. Moyal curves were fitted to the distribution of the charges as Moyal curves are effective approximations of Landau distributions [11]. In more detail, Landau distributions are probability density functions that describe the distributions of energy loss of a charged particle passing through a medium [10]. Therefore, Landau distributions, along with the Moyal curve approximations, are capable of describing the distribution of charges of incoming muons passing through the steel layers. The equation for a Moyal curve,  $g_z(x)$ , is expressed as:

$$g_z(x) = \frac{1}{\sqrt{2\pi}\sigma} e^{-\frac{1}{2}\left[\frac{x-\mu}{\sigma} + e^{-\frac{x-\mu}{\sigma}}\right]}, \quad (6)$$

where  $\mu$  is the location parameter and  $\sigma$  is the scale parameter for a random value  $x$  in the probability distribution.

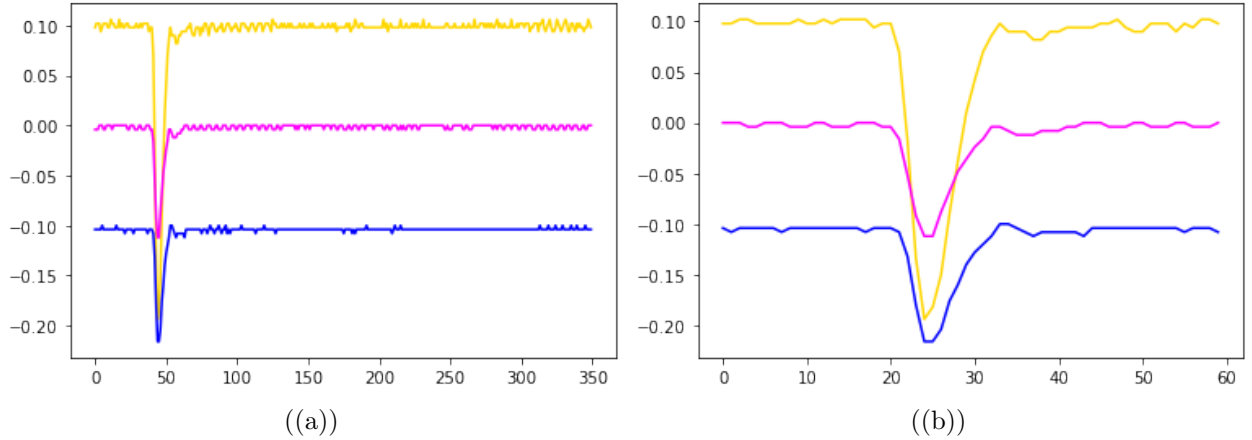


Figure 1: Sample traces for setup used to calibrate scintillator A at 15V. a) Total area recorded from oscilloscope. b) Close-up of integrated area that was included into the distribution of charges.

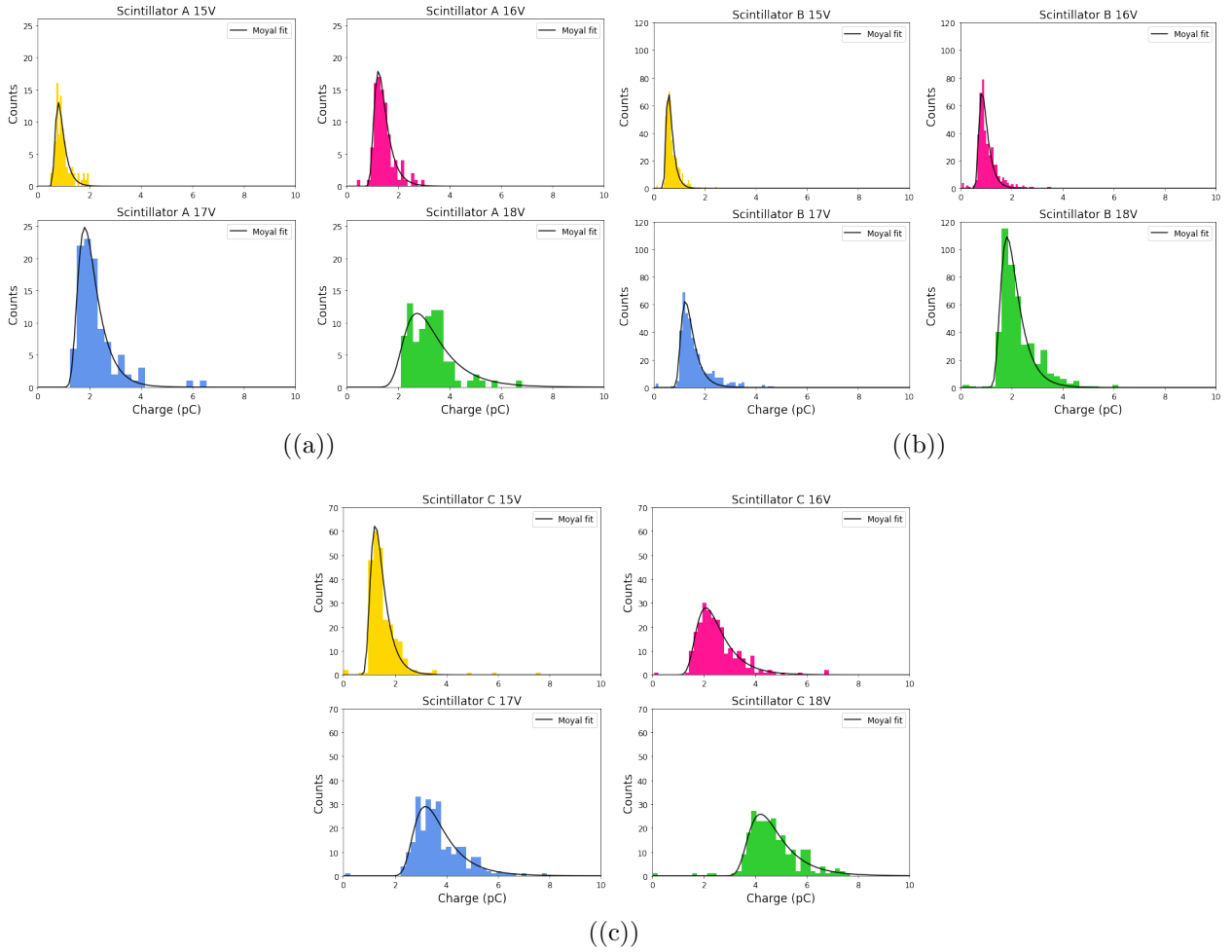


Figure 2: Landau distributions of charges in pC for voltages of 15V, 16V, 17V, and 18V, along with Moyal fit created through curve fitting expressed through equation (6). a). Distribution of charges for scintillator A with sample of size  $n = 500$  for all graphs. b). Distribution of charges for scintillator B with sample of size  $n = 1000$  for all graphs. c.) Distribution of charges for scintillator C with sample of size  $n = 500$  for all graphs.

## 2.2 Experimental Design

The experimental design used to measure muon lifetimes featured the three detectors stacked on top of each other in the order of A, B, and C from top to bottom with steel layers between them, as seen in Figure 3. The first steel layer has the purpose of slowing down incoming muons, which have a broad spectrum of energies, so that more would stop in the second layer. Afterward, muons absorbed by the second steel layer would decay and emit an electron, which would pass through detectors B or C, depending on the direction it was emitted in the decay.

Hence, the coincidence logic for this experiment is  $A \cdot B \cdot \bar{C}$  for the trigger and  $\bar{A} \cdot (B + C)$  for an event.

The data was taken using a SDS1204X-E SIGLENT oscilloscope connected to a laptop running a Python program, and the data analysis was performed on the raw data. The muon lifetime was calculated by taking the time difference between the activation of the trigger on the oscilloscope and the detection of the electron due to muon decay. Only a pulse from detector B was required to trigger the oscilloscope, and the complete trigger logic was applied to the offline analysis. The analysis was performed using a Python program using the Numpy and Matplotlib modules.

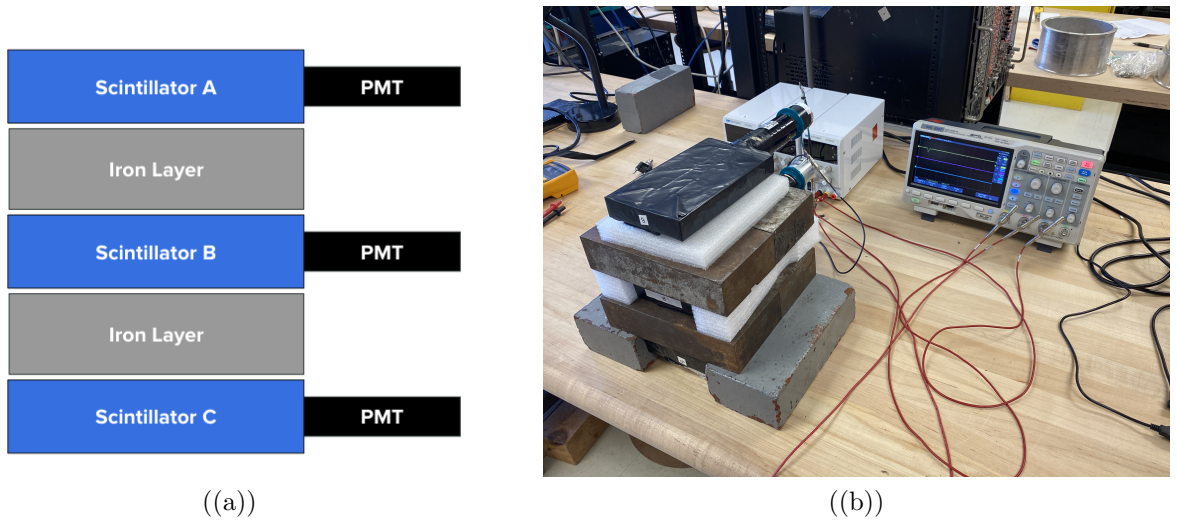


Figure 3: Experimental setup of muon detectors A, B, and C along with steel layers as stopping media. a) Diagram of the apparatus. b) Image of the apparatus in the lab.

### 3 Results

Data collection for muon lifetimes was performed for six days using the SDS1204X-E SIGLENT oscilloscope. Each data file used for this experiment contained no more than 3000 traces to ensure that the Python program did not face memory issues when performing the data analysis. A total of 189,000 traces were recorded during this period. Within this data, 178 muon decays were observed. The traces of a muon decay illustrating the logic of the experiment are shown in Figure 4.

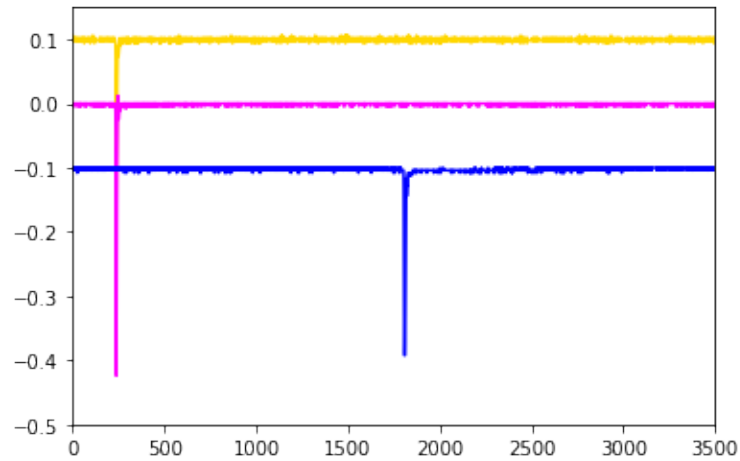


Figure 4: Sample of traces where there are incoming pulses on detectors A and B and a decay electron on detector C.

The distribution of the measured lifetimes for the decays is shown in Figure 5, along with an exponential fit created using the Curve Fit module imported from the SciPy Python library. Extracting the mean of the lifetime distributions, an average muon lifetime of  $\tau = 2.18 \pm 0.3 \mu\text{s}$  is obtained.

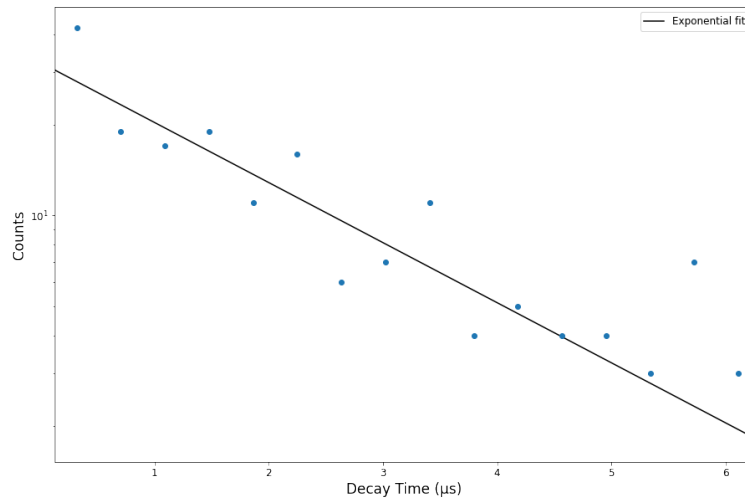


Figure 5: Distribution of muon lifetimes with error bars,  $\tau$ , in microseconds along with exponential fit created through curve fitting expressed by equation (5) and represented with a logarithmic vertical axis.



## 4 Discussion

Taking note that the accepted value for the lifetime of a muon is calculated at  $\tau = 2.1969811 \pm 0.0000022 \mu\text{s}$  [6], it is possible to affirm that the calculated value obtained from this experiment,  $\tau = 2.18 \pm 0.3 \mu\text{s}$ , is in agreement with the accepted value within  $1 \sigma$ . This result demonstrates that the measured value of  $\tau$  is following the accepted value and, by proxy, that the muon lifetime was successfully calculated. This is further highlighted by a qualitative analysis of Figure 5, given that the data distribution demonstrates a pattern of exponential decay, which is expected as muon decays, like any other type of radioactive decay, will tend to follow an exponential decay pattern [12]. On the other hand, it is essential to note that Figure 5 may present a pedestal around values nearing zero, which could be due to a source of error in the experimental design and be responsible for skewing the results.

Moreover, it must be remarked that some issues were encountered during the data collection as a data file of 100,000 traces was too large to be analyzed by the Python program; this issue, however, was overcome by separating the larger file into separate files each of which contained 3,000 traces. The Python program was then adjusted to record 3,000 traces in each data file to prevent memory issues during data analysis.

## 5 Conclusion

This study concludes that the experimental setup successfully measured muon lifetimes within  $1 \sigma$  of the accepted value with a measured value of  $\tau = 2.18 \pm 0.3 \mu\text{s}$ . By accurately measuring muon lifetimes, this study shows excellent capacity in characterizing elementary particles, which is a powerful tool for obtaining universal constants. Furthermore, this study demonstrates that muon lifetime distributions follow standard exponential decay rates. Therefore, future studies should consider collecting a higher number of traces with the hopes of increasing experimental accuracy by detecting a higher number of events.

## 6 Acknowledgments

The author of this report would like to thank Prof. David Hanna and Dr. Stephan O'Brien for providing the necessary supervision, feedback, and infrastructure on all the steps of the project. Furthermore, this project counted with the valuable contributions of Mr. Fadi Younes, who provided the statistical analysis program used in the calculation of muon lifetimes.

## References

- [1] C. D. Anderson, & S. H. Neddermeyer, "Cloud Chamber Observations of Cosmic Rays at 4300 Meters Elevation and Near Sea-Level," *Physical Review*, vol. 50, no. 4, pp. 263–271, 1936. [Accessed May 27 2022] [1](#)
- [2] D. Lal, & B. Peters, *Cosmic Ray Produced Radioactivity on the Earth*. Berlin & Heidelberg, Germany: Springer, 1967. [Accessed May 30 2022] [1](#)
- [3] B. Rossi, *High-Energy Particles*. New York, United States of America: Prentice-Hall, 1952. [Accessed May 27 2022] [1](#)
- [4] J. D. Walecka, "Semi-leptonic weak and electromagnetic interactions with nuclei: Muon capture to discrete nuclear levels from hyperfine states," *Nuclear Physics A*, vol. 258, no. 3, pp. 397–416, 1976. [Accessed June 17 2022] [1](#)
- [5] A. Knecht, A. Skawran, & S. M. Vogiatzi, "Study of nuclear properties with muonic atoms," *The European Physical Journal Plus*, vol. 135, no. 10, 2020. [Accessed June 17 2022] [1](#)
- [6] R.L. Workman, et al. (Particle Data Group), to be published (2022) [Accessed May 27 2022] [1](#), [8](#)
- [7] D. F. Measday, "The nuclear physics of muon capture," *Physics Reports*, vol. 354, no. 4-5, pp. 243–409, 2001. [Accessed June 1 2022] [2](#)
- [8] E. Fermi, & E. Teller, "The Capture of Negative Mesotrons in Matter," *Physical Review*, vol. 72, no. 5, pp. 399–408, 1947. [Accessed June 1 2022] [2](#)
- [9] W. R. Leo, *Techniques for Nuclear and Particle Physics Experiments*. Berlin & Heidelberg, Germany: Springer, 1994. [Accessed June 3 2022] [3](#)
- [10] L. Landau, "On the energy loss of fast particles by ionization," *Journal of Physics*, vol. 8, no. 4, pp. 201–205, 1944. [Accessed June 3 2022] [4](#)

- [11] J. E. Moyal, "Theory of ionization fluctuations," *The London, Edinburgh, and Dublin Philosophical Magazine and Journal of Science*, vol. 46, no. 374, pp. 263–280, 1955. [Accessed June 4 2022] [4](#)
- [12] E. Rutherford, & F. Soddy, "Radioactive Change," *The London, Edinburgh, and Dublin Philosophical Magazine and Journal of Science*, vol. 5, no. 29, pp. 576–591, 1903. [Accessed June 4 2022] [8](#)

## A Plotted Means for Scintillator Calibration

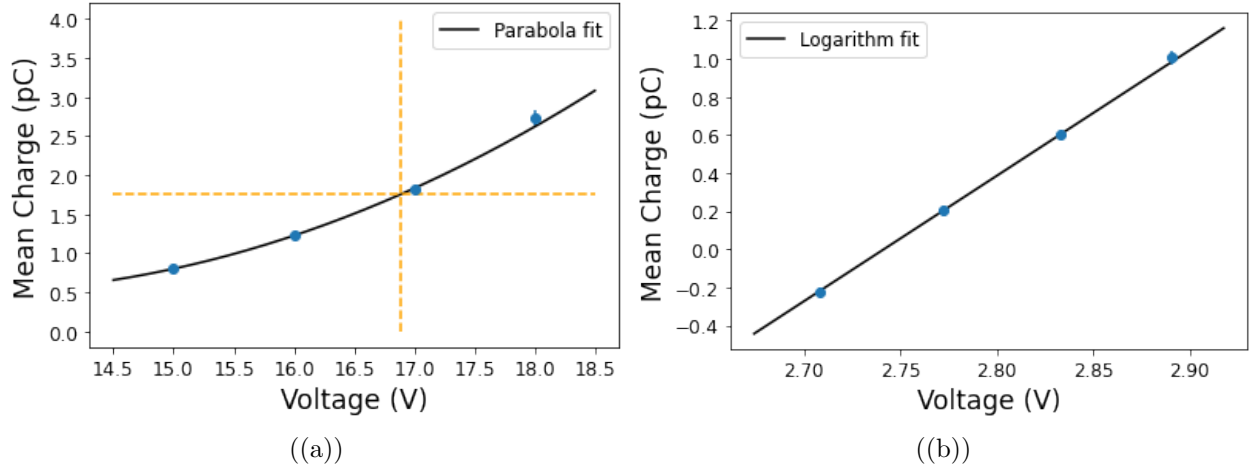


Figure 6: Plotted mean charges for scintillator A used for high-voltage calibration. a) Plotted means with a parabola fit, orange cross centered at point in the parabola that yields a mean charge of 1.75 pC. b) Plotted means with logarithmic scaling and appropriate linear fit.

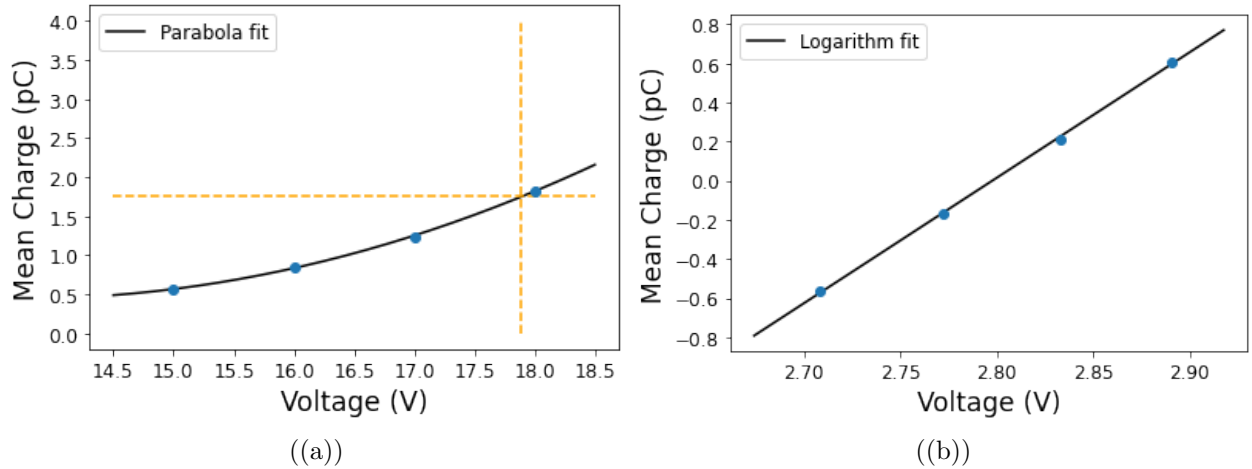


Figure 7: Plotted mean charges for scintillator B used for high-voltage calibration. a) Plotted means with a parabola fit, orange cross centered at point in the parabola that yields a mean charge of 1.75 pC. b) Plotted means with logarithmic scaling and appropriate linear fit.

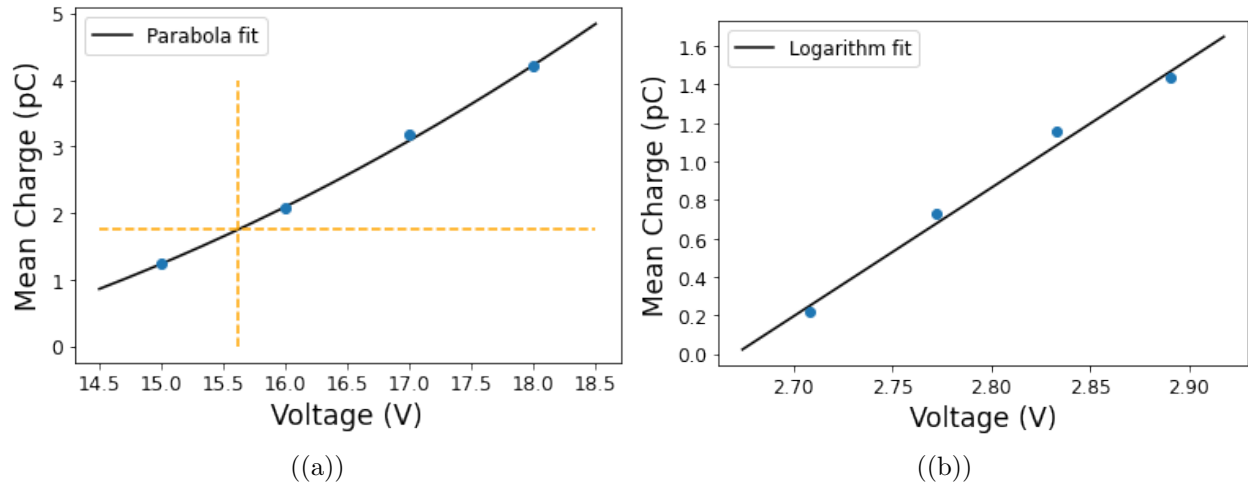


Figure 8: Plotted mean charges for scintillator C used for high-voltage calibration. a) Plotted means with a parabola fit, orange cross centered at point in the parabola that yields a mean charge of 1.75 pC. b) Plotted means with logarithmic scaling and appropriate linear fit.